Applied Energy 183 (2016) 645–658

Contents lists available at ScienceDirect

Applied Energy

journal homepage: www.elsevier.com/locate/apenergy

Sizing for fuel cell/supercapacitor hybrid vehicles based on stochastic driving cycles

Diego Feroldi [a,b,*], Mauro Carignano [c]

[a] CIFASIS-CONICET-UNR, Rosario, Argentina
[b] Department of Computer Sciences, FCEIA-UNR, Rosario, Argentina
[c] Department of Mechanical Engineering, FCEIA-UNR, CONICET, Rosario, Argentina

HIGHLIGHTS

- A sizing procedure based on the fulfilment of real driving conditions is proposed.
- A methodology to generate long-term stochastic driving cycles is proposed.
- A parametric optimization of the real-time EMS is conducted.
- A trade-off design is adopted from a Pareto front.
- A comparison with optimal consumption via Dynamic Programming is performed.

ARTICLE INFO

Article history:
Received 2 June 2016
Received in revised form 2 September 2016
Accepted 3 September 2016
Available online 13 September 2016

Keywords:
Fuel cell vehicles
Hybrid systems
Energy management strategy
Stochastic driving cycle
Supercapacitors

ABSTRACT

In this article, a methodology for the sizing and analysis of fuel cell/supercapacitor hybrid vehicles is presented. The proposed sizing methodology is based on the fulfilment of power requirements, including sustained speed tests and stochastic driving cycles. The procedure to generate driving cycles is also presented in this paper. The sizing algorithm explicitly accounts for the Equivalent Consumption Minimization Strategy (ECMS). The performance is compared with optimal consumption, which is found using an off-line strategy via Dynamic Programming. The sizing methodology provides guidance for sizing the fuel cell and the supercapacitor number. The results also include analysis on oversizing the fuel cell and varying the parameters of the energy management strategy. The simulation results highlight the importance of integrating sizing and energy management into fuel cell hybrid vehicles.

1. Introduction

Fuel cell/supercapacitor hybrid vehicles are a promising alternative for efficient and clean propulsion. This type of hybrid vehicles exploits the advantages of both Polymer Electrolyte Membrane Fuel Cells (FCs) and supercapacitors. FCs have several advantages, including high efficiency, low-temperature operation, and are clean functioning (the only by-products are heat and water). These characteristics make FCs an excellent option for vehicles, mainly in urban environments where the problem of air pollution is more severe. However, the dynamics of FCs are relatively slow, primarily because of the dynamics of the air compressor and manifold-filling dynamics [1]. Alternatively, supercapacitors are able to store energy with high specific power but low specific energy. The presence of an Energy Storage System (ESS) in the hybrid topology provides a helpful way to operate the powertrain efficiently because the power generation may be decoupled from the load. This means that the fuel cell can be used at a more convenient point of operation, while the supercapacitors absorb or supply the remaining power to meet power requirements. The fuel cell operating point is determined by the Energy Management Strategy (EMS).

Several approaches are reported in the literature for sizing and energy management in fuel cell hybrid vehicles (FCHV). However, most of them address these issues separately despite the deep interrelationship between them. In [2], an integrated optimization approach for component sizing and energy management is presented. However, the EMS that was employed is a rule-based strategy. With regard to sizing, some approaches are oriented to optimize design parameters based on standard driving cycles. Although standard driving cycles are extremely important for evaluating the performance of FCHVs, it is necessary that the design ensures the fulfilment of specific drivability requirements.

* Corresponding author at: CIFASIS-CONICET-UNR, Rosario, Argentina.
E-mail address: feroldi@cifasis-conicet.gov.ar (D. Feroldi).

http://dx.doi.org/10.1016/j.apenergy.2016.09.008
0306-2619/

Nomenclature

Greek letters

α	road slope [%]
α_s	road slope in Test 2 [%]
γ_{FC}	weight-to-power ratio of the fuel cell [kg kW^{-1}]
$\Delta P_{FC,min}$	minimum fuel cell fall rate [W s^{-1}]
$\Delta P_{FC,max}$	maximum fuel cell rise rate [W s^{-1}]
Δt	sampling time [s]
δ_{v_t}	tolerance band
η_B	efficiency of the boost converter [–]
$\eta_{B/B}$	efficiency of the buck/boost converter [–]
η_{GB}	efficiency of the gear box [–]
$\eta_{g,FC}$	global efficiency of the FC [–]
$\eta_{g,Prop}$	global efficiency of the propulsion system [–]
η_{SC}	efficiency of the supercapacitor bank [–]
η_{FC}	efficiency of the fuel cell [–]
η_{inv}	efficiency of the inverter [–]
η_m	efficiency of the electric motor [–]
ρ	air density [kg m^{-3}]

Upper cases

AR	Artemis Road driving cycle
AU	Artemis Urban driving cycle
AC	alternating current
A_F	frontal area of the vehicle [m^2]
Br/H$_2$	braking/hydrogen ratio [%]
C_{AD}	aerodynamic drag coefficient of the vehicle [–]
C_v	speed compliance [%]
C_{v_t}	speed compliance target [%]
CDC	Combined Driving Cycle
C_{H_2}	hydrogen consumption [g s^{-1}]
C_{RR}	rolling resistance coefficient [–]
DC	direct current
$E_{SC,max}$	capacity of the supercapacitor modules [Wh kg^{-1}]
ECMS	Equivalent Consumption Minimization Strategy
EMS	Energy Management Strategy
ESS	Energy Storage System
FCHV	Fuel Cell Hybrid Vehicle
H_2	hydrogen
$H_{2,cons}$	normalize hydrogen consumption [g km^{-1}]
HEV	Hybrid Electric Vehicle
HWFET	Highway Fuel Economy Test driving cycle
L	length of the driving cycle [–]
LHV$_{H_2}$	Lower Heating Value of hydrogen
N_{SC}	number of supercapacitor modules [–]
$N_{SC,max}$	maximum number of supercapacitor modules [–]
$N_{SC,min}$	minimum number of supercapacitor modules [–]
MT	microtrip
MI	microidle
N_{ms}	number of missed-speeds [–]
P_{AD}	power to overcome the air resistance [W]
P_{acc}	power required to accelerate [W]
P_{FC}	fuel cell power [W]
$P_{FC,i}$	fuel cell power in Test i [W]
$P_{FC,max}$	fuel cell maximum power [W]
$P_{FC,min}$	fuel cell minimum power [W]
$P_{FC,ref}$	reference for the fuel cell power [W]
P_g	power required to climb a slope [W]
P_{load}	power consumed by the load [W]
P_{req}	power required to the powertrain [W]
P_{roll}	power required to overcome the rolling resistance [W]
$P_{SC,lim}$	power limit of the supercapacitor bank [W]
SC	supercapacitor
SDC	Stochastic Driving Cycle
SOC	state of charge of the supercapacitor bank [–]
SOC_{ref}	reference SOC [–]
SOC_{max}	maximum SOC [–]
SOC_{min}	minimum SOC [–]
UDDS	Urban Dynamometer Driving Cycle
$V_{SC,min}$	SC minimum voltage [V]
$V_{SC,max}$	SC maximum voltage [V]
$V_{SC,oc}$	SC open circuit voltage [V]

Lower cases

a	acceleration of the vehicle [m s^{-2}]
a_i	polynomial coefficients
b_i	polynomial coefficients
c_i	polynomial coefficients
g	gravity acceleration [m s^{-2}]
k_s	scale variable [–]
m_c	cargo mass [kg]
$m_{v,b}$	base mass of the vehicle (without including the fuel cell or the SC mass) [kg]
m_v	total vehicle mass [kg]
m_{FC}	mass of the fuel cell [kg]
m_{SC}	mass of a supercapacitor module [kg]
v	speed of the vehicle [km h^{-1}]
s_i	parameter in ECMS [–]
v_{si}	sustained speed in Test i [km h^{-1}]
u	control input vector

Moreover, some sizing approaches are based on drivability requirements [3,4]. These methods are robust and compatible with industry requirements. In contrast, other approaches propose methodologies where a minimization problem is solved. For example, in some studies [5,6], component sizing is determined within a feasible region based on Pontryagin's minimum principle. Other works address a multi-objective optimization problem, obtaining a quasi-optimal solution [7–9]. Optimization with multi-objective genetic algorithms can also be used [10], while convex programming has been applied successfully in some works concerning sizing and energy management [11,12].

The energy management can be divided into two classes: heuristic and optimization approaches [13]. EMS for fuel cell-based hybrid electric vehicles (HEVs) in combination with a battery and/or supercapacitors has been reviewed [14]. An important conclusion was that the combination of the fast transient response of supercapacitors and the slow transient response of fuel cells is an attractive alternative for improving the efficiency and performance of HEVs. The optimization approach based on the Equivalent Consumption Minimization Strategy (ECMS) has important advantages, that allow it be used in real-time [15–17].

Previous studies have used other optimization techniques. Model predictive control oriented towards energy management has been used [18]. In [19], a stochastic self-optimizing power management strategy for a fuel cell/battery-powered hybrid electric scooter is proposed. In [20], an improved dynamic programming approach is presented, where several look-up tables are constructed to permit online operation. Alternately, approaches based on rules or heuristics can be more appropriate for real-time application [21–26]. Fuzzy logic is another heuristic approach used in some works [27–29].

From the literature, despite the many existing approaches, the sizing issue is generally addressed, assuming some critical considerations in view of real applications. These assumptions include

using synthesized driving cycles or using only one standard driving cycle to evaluate the performance, using offline EMS to perform the power split, and not considering the power rate constraints of FCs.

In this paper, a sizing methodology for a fuel cell/supercapacitor hybrid vehicle is proposed. The methodology is based on the fulfilment of driving requirements, which include sustained speed tests and simulations under real driving cycle conditions. The sizing methodology is integrated with the EMS. The EMS employed is the widely used Equivalent Consumption Minimization Strategy (ECMS), whose parameters are adjusted during the sizing procedure. The proposed sizing methodology allows one to find the size of the FC and the number of SC modules that fulfil several driving conditions, minimizing hydrogen consumption. The considered driving cycle is generated through a stochastic procedure, which is also presented in this paper. Moreover, to evaluate the performance of the ECMS, the optimal hydrogen consumption is determined offline through deterministic dynamic programming. The methodology proposed and the analysis of the results presented are general enough to cover a wide range of real applications.

The paper is organized as follows. In Section 2, a description of the model of the fuel cell hybrid vehicle is provided. In Section 3, the generation of stochastic driving cycles is addressed. In Section 4, the energy management strategy used in the sizing process is introduced. In Section 5, the sizing methodology is proposed. The results are presented and discussed in Section 6, while the conclusions are presented in Section 7.

2. Fuel cell hybrid vehicle model

The Fuel Cell Hybrid Vehicle (FCHV) is powered by an FC. The powertrain also includes an ESS, which is composed of a supercapacitor bank. The powertrain configuration is depicted in Fig. 1. This is a series configuration where the electric motors can be fed from both the FC and ESS. The hybrid topology also has three power converters that provide the voltage level required for the power conversion. A power converter is used to boost the voltage from the fuel cell output to the direct current (DC) bus. A buck/boost converter is used to allow the bidirectional energy flow between the DC bus and the supercapacitor bank. There is also a power inverter for alternating current (AC) loads.

The ESS can be charged from both the FC and the load. The first case can appear when the FC supplies more power than the load requirement. This is known as the charging mode. The second case is when the vehicle is in the regenerative braking mode. Regenerative braking is defined as the process that captures the kinetic energy from a moving car when it is in a coasting or braking mode [13].

The main component of the FC is a fuel cell stack, whose anode is fed with hydrogen from a pressurized tank and cathode is fed with air through an air compressor. The FC in this work is modelled through an efficiency and hydrogen consumption map as a function of the fuel cell power (P_{FC}):

$$\eta_{FC} = f(P_{FC}), \tag{1}$$
$$C_{H_2} = h(P_{FC}), \tag{2}$$

where η_{FC} and $\dot{h}_{FC}$ are the efficiency and the hydrogen consumption of the FC, respectively. The fuel cell efficiency and the hydrogen consumption maps used in this work are linearly scaled using the data of a 50-kW FC model from ADVISOR [30].

The hydrogen consumption map and the efficiency map can be approximated by two third-order polynomials, as observed from Fig. 2. Therefore, hydrogen consumption and efficiency can be expressed as:

$$C_{H_2}(k) = a_3 P_{FC}^3(k) + a_2 P_{FC}^2(k) + a_1 P_{FC}(k) + a_0, \tag{3}$$
$$\eta_{FC}(k) = b_3 P_{FC}^3(k) + b_2 P_{FC}^2(k) + b_1 P_{FC}(k) + b_0. \tag{4}$$

This model is simple enough to be used in the context of the sizing methodology and the energy management strategy, as presented in [21].

The model of the vehicle is also simplified for use with the same objectives. The power consumed by the load can be expressed as the sum of the power required to accelerate (P_{acc}), the power required to overcome the rolling resistance (P_{roll}), the power to overcome the air resistance (P_{AD}), and the power required to climb a slope (P_g) [31,32]:

$$P_{load}(k) = P_{roll}(k) + P_{AD}(k) + P_{acc}(k) + P_g(k), \tag{5}$$

where k (with $k = 0, 1, 2, \ldots$) is the index of the time steps. The powers in (5) are defined as follows:

$$P_{acc}(k) = m_v\, a(k)\, v(k), \tag{6}$$
$$P_{roll}(k) = C_{RR}\, m_v\, g\, v(k)\, \cos(\alpha(k)), \tag{7}$$
$$P_{AD}(k) = 0.5\, \rho\, C_{AD}\, A_F\, v(k)^3, \tag{8}$$
$$P_g(k) = m_v\, g\, \sin(\alpha(k))\, v(k), \tag{9}$$

where m_v is the vehicle mass, v is the vehicle speed, a is the acceleration, C_{RR} is the rolling resistance coefficient, g is the gravity acceleration, ρ is the air density, C_{AD} is the aerodynamic drag coefficient of the vehicle, A_F is the frontal area of the vehicle, and α is the road slope. The vehicle mass can be expressed as follows:

$$m_v = m_{v,b} + m_c + P_{FC,\max}\, \gamma_{FC} + N_{SC} m_{SC}, \tag{10}$$

where $m_{v,b}$ is the base mass of the vehicle (without the fuel cell or the SC bank), m_c is the cargo mass, $P_{FC,\max}$ is the maximum power of

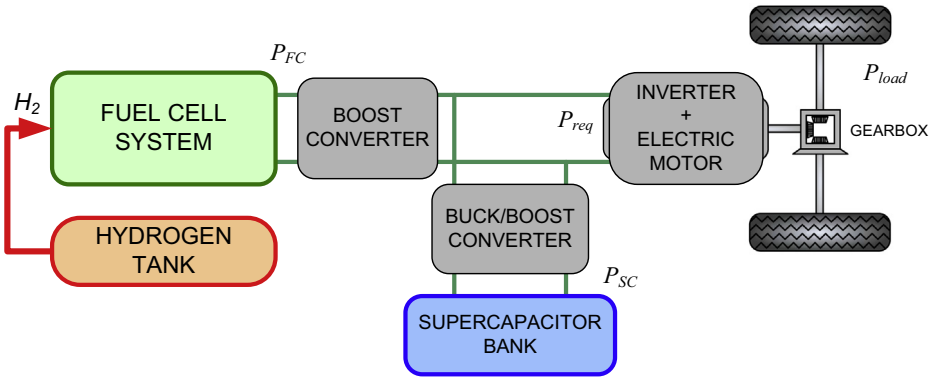

Fig. 1. Block diagram of the fuel cell hybrid vehicle.

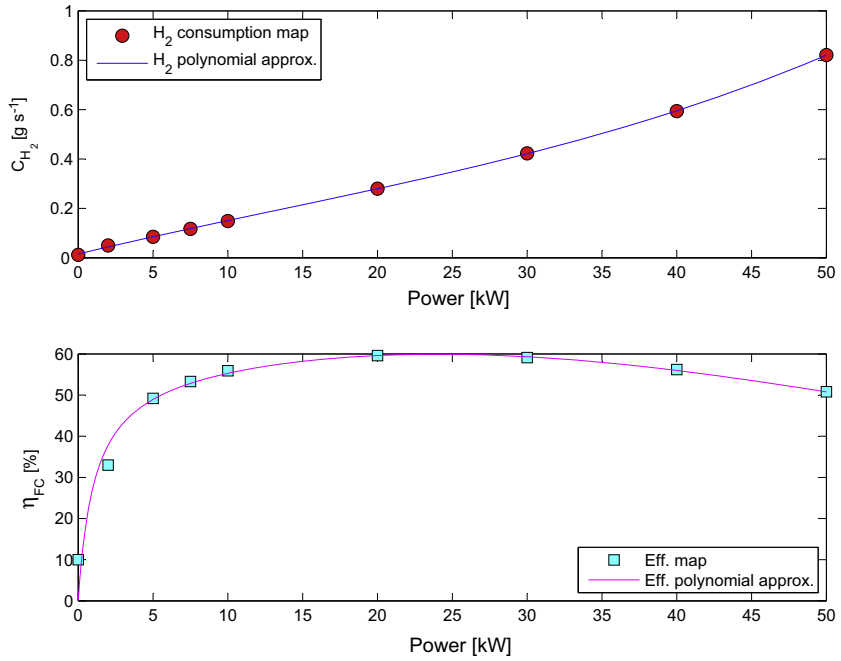

Fig. 2. Polynomial approximation for the FC efficiency and hydrogen consumption maps for a 50-kW FC.

the FC, γ_{FC} is the weight-to-power ratio of the FC, N_{SC} is the number of supercapacitors, and m_{SC} is the mass of each supercapacitor module.

The acceleration in (6) is calculated as the change in speed during the time increment divided by the sampling time (Δt):

$$a(k) = \frac{v(k) - v(k-1)}{\Delta t}. \tag{11}$$

The required power to the DC bus is higher than P_{load} due to the losses in the gearbox, the electric motor, and the electrical inverter. Moreover, some power is dissipated as friction from the brakes (P_{br}). Thus, the required power (P_{req}) that results is:

$$P_{req}(k) = \frac{P_{load}(k) - P_{br}(k)}{\tilde{\eta}}, \tag{12}$$

with $\tilde{\eta} = \eta_{GB}\,\eta_m\,\eta_{inv}$, where η_{GB}, η_m, and η_{inv} are the efficiencies of the gearbox, the motor, and the electrical inverter, respectively, and are assumed to be constant.

Supercapacitors are energy storage elements with high specific power. The more relevant applications of supercapacitors are those that require many fast charge/discharge cycles, such as automotive applications where power peaks and regenerative braking are frequent. Furthermore, supercapacitors have high efficiency. The efficiency of the supercapacitors considered in this paper is 99% [30]. Other important characteristics of the supercapacitor modules are their very low internal resistance and capacity.

The dynamics of the State of Charge (SOC) of the supercapacitor bank can be modelled by the following equation:

$$\mathrm{SOC}(k+1) = \mathrm{SOC}(k) + \Delta\mathrm{SOC}(k), \tag{13}$$

with

$$\Delta\mathrm{SOC}(k) = \frac{P_{SC}(k)\,\Delta t}{(\eta_{SC})^{sign(P_{SC}(k))}\,E_{SC,\,bank}}, \tag{14}$$

where

$$E_{SC,\,bank} = N_{SC}\,m_{SC}\,E_{SC,max}\,3600 \tag{15}$$

is the capacity of the SC bank, η_{SC} [−] is the efficiency of the SC bank, P_{SC} [W] is the power from the SC bank, and m_{SC} [kg] and $E_{SC,max}$ [Wh kg^{-1}] are the mass and the specific capacity of each module. By convention, P_{SC} is negative when charging and positive when discharging.

The power of the supercapacitor bank is limited, based on the SOC. The limits are the following, provided that the supercapacitors are connected in series:

$$P_{SC,\,lim}(k) = \begin{cases} \frac{N_{SC}\,V_{SC,\,max}\left(V_{SC,\,oc}(k) - V_{SC,\,max}\right)}{r_i} & \text{when charging,} \\ \frac{N_{SC}\,V_{SC,\,min}\left(V_{SC,\,oc}(k) - V_{SC,\,min}\right)}{r_i} & \text{when discharging,} \end{cases} \tag{16}$$

where $V_{SC,\,max}$ and $V_{SC,\,min}$ are the maximum and minimum voltage limits of the supercapacitors, r_i is the internal resistance, and $V_{SC,\,oc}$ is the open-circuit voltage at a given value of SOC, which can be approximated by the following affine function:

$$V_{SC,\,oc}(k) = c_1\,\mathrm{SOC}(k) + c_0, \tag{17}$$

where $V_{SC,\,oc}$ is in volts and SOC is dimensionless, with $\mathrm{SOC}(k) = 1$ for a fully charged supercapacitor. The values of these parameters correspond to a supercapacitor model from ADVISOR [30].

The values of all the parameters mentioned in this section are listed in Table 1 [30], which represent an average light car, while $P_{FC,\,max}$ and N_{SC} result from the sizing procedure presented in Section 5.

3. Stochastic driving cycle

A driving cycle is a set of data points representing vehicle speed versus time [33]. There is a particular interest in standard driving cycles because they offer the possibility of comparing results. However, standard cycles only account for certain, precise conditions and may not always be representative of real-world driving conditions [34]. In addition, a large number of studies dealing with hybrid vehicles use either just one driving cycle or a very small number of driving cycles [35]. Therefore, long-term stochastic

Table 1
Parameter of the vehicle model.

Parameter	Symbol	Value
Base vehicle mass	$m_{v,b}$	882 kg
Cargo mass	m_c	80 kg
Gravity acceleration	g	9.8 m s^{-2}
Air density	ρ	1.2 kg m^{-3}
Rolling resistance coefficient	C_{RR}	0.014
Drag coefficient	C_{AD}	0.3
Front area	A_F	1.746 m^2
SC mass	m_{SC}	0.408 kg
SC specific capacity	$E_{SC,max}$	6 W h kg^{-1}
SC internal resistance	r_i	0.206 mΩ
SC maximum voltage	$V_{SC,max}$	3 V
SC minimum voltage	$V_{SC,min}$	1 V
FC weight-to-power ratio	γ_{FC}	3 kg kW^{-1}
Boost converter efficiency	η_B	0.95
Buck/boost converter efficiency	$\eta_{B/B}$	0.95
Inverter efficiency	η_{inv}	0.95
Supercapacitors efficiency	η_{SC}	0.99
Electric motor efficiency	η_m	0.95
Gear box efficiency	η_{GB}	0.9

driving cycles that consider a multitude of different driving conditions can overcome this drawback.

The stochastic driving cycles in this work are generated from standard driving cycles. The standard driving cycles considered in this methodology are the following: Urban Dynamometer Driving Schedule (UDDS), Highway Fuel Economy Cycle (HWFET), Artemis Urban (AU), and Artemis Road (AR) [36]. The selected driving cycles cover a broad range of driving conditions (urban, suburban, and highway) for passenger cars.

The first step in the proposed methodology for obtaining the stochastic driving cycle (SDC) is to generate a combined driving cycle (CDC), which is the result of the concatenation of the four aforementioned standard driving cycles. Then, the SDC is generated from a CDC through the methodology explained below. The SDC is not dependent on a particular driving cycle, but it has similar properties to those of the cycles used in the generation process. Some relevant statistical metrics of the driving cycles are shown in Table 2, where the cruise time is defined as a time in which the speed is greater than 0.3 m s^{-1} and the acceleration is less than ±0.03 m s^{-2}, the mean run speed is defined as the average speed excluding the idle period, the acceleration time is defined as the amount of time with an acceleration greater than 0.03 m s^{-2}, and the deceleration time is defined as the amount of time with an acceleration lower than −0.03 m s^{-2} [37].

The second step in the methodology is to search for microtrips and microidles from the CDC. A microtrip (MT) is defined as a segment of the cycle where the speed is non-zero. On the contrary, a microidle (MI) is defined as a segment where the speed is equal to zero [38]. Fig. 3 illustrates the concept of microtrips and microidles.

Once the set of MTs and MIs are collected, the SDC is generated by alternately adding MIs and MTs through a random process until the length is greater than the value of L. In addition, each MI and MT is scaled. The scaling of an MI is according to the length while the scaling of the MT is according to the speed values. In both cases, the scaling is linear using a variable scale k_s, chosen randomly (with uniform distribution) within a defined range: $k_s \in [0.8, 1.2]$. After scaling an MT, three constraints must be verified: the maximum and minimum allowable acceleration and the maximum allowable speed. If the constraints are not satisfied, the scaling process is repeated until the constraints are satisfied. In this manner, generating an SDC that is more demanding than the CDC is avoided. The procedure previously explained is summarized in the flow chart depicted in Fig. 4.

Finally, once an SDC has been constructed, a validation is performed. Two analysis methods have been incorporated to assess these new driving cycles. First, the generated SDC has been validated by comparison with the statistical metrics in Table 2. In addition, Figs. 5 and 6 show the speed probability diagram and the acceleration probability diagram, respectively. The results indicate that the generated cycle is accurate and that it is not skewed to a specific speed or acceleration.

4. Energy management strategy

The objective of the EMS is to determine the operation point of the fuel cell to (i) meet power requirements (drivability); (ii) operate the components within their limits; and (iii) maximize the global efficiency. Typically, the EMS has a great impact on the efficiency of the HEV, but the drivability is mainly limited by the size of the components. However, when the powertrain is composed by an SC bank and an FC, constraints associated with the SOC in the ESS and with the power rates in the FC are frequently activated during operation. Therefore, in this type of HEV, the EMS takes on an even greater importance for drivability.

The power balance, according to Fig. 1 and (12), can be expressed as follows:

$$P_{load}(k) = (P_{FC}(k)\,\eta_B + P_{SC}(k)\,\eta_{B/B})\,\tilde{\eta} + P_{br}(k), \tag{18}$$

Table 2
Properties of the driving cycles.

Property	UDDS	HWFET	AU	AR	CDC	SDC
Duration [s]	1370	766	993	1082	4211	50048
Acceleration time [s]	541	312	374	489	1716	20240
Deceleration time [s]	482	267	349	449	1547	18,207
Idle time [s]	242	5	260	29	536	7335
Cruise time [s]	992	577	674	926	3169	37,170
Distance [km]	11.990	16.507	4.870	17.272	50.639	541.280
Maximum speed [km h^{-1}]	91.3	96.4	57.5	111.1	111.1	110.9
Average speed [km h^{-1}]	31.5	77.6	17.7	57.5	43.3	38.93
Average run speed [km h^{-1}]	38.3	78.1	23.9	59.1	49.6	45.6
Standard deviation of speed [km h^{-1}]	23.6	16.5	16.9	24.5	30.3	29.1
Maximum acceleration [m s^{-2}]	1.48	1.43	2.44	2.04	2.44	2.83
Average acceleration [m s^{-2}]	0.480	0.18	0.65	0.42	0.44	0.45
Maximum deceleration [m s^{-2}]	−1.48	−1.48	−2.8	−3.76	−3.76	−3.70
Average deceleration [m s^{-2}]	−0.53	−0.200	−0.70	−0.46	−0.48	−0.50
Standard deviation of acceleration [m s^{-2}]	0.4	0.21	0.49	0.38	0.42	0.43

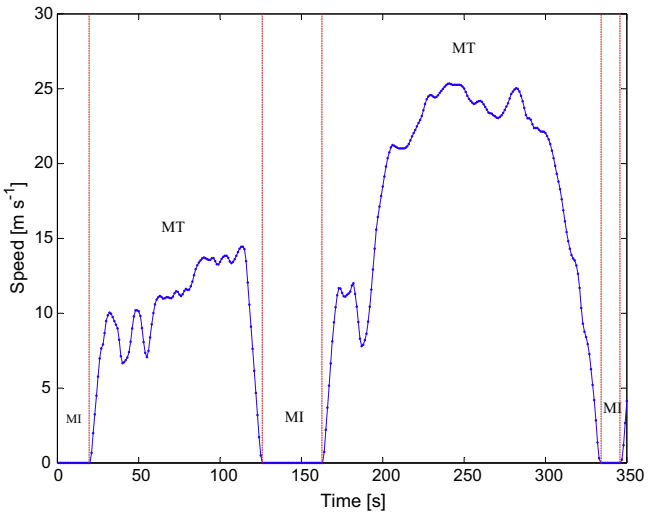

Fig. 3. Illustrative example of microtrips (MTs) and microidles (MIs).

where $\eta_{B/B}$ is the efficiency of the Buck/Boost power converter. In addition, the power balance (18) is subject to the following constraints:

$$P_{FC,min} \leqslant P_{FC}(k) \leqslant P_{FC,max}, \tag{19}$$

$$\Delta P_{FC,min} \leqslant \Delta P_{FC}(k) \leqslant \Delta P_{FC,max}, \tag{20}$$

$$P_{SC,min}(k) \leqslant P_{SC}(k) \leqslant P_{SC,max}(k), \tag{21}$$

$$SOC_{min} \leqslant SOC(k) \leqslant SOC_{max}, \tag{22}$$

where

$$\Delta P_{FC}(k) = P_{FC}(k) - P_{FC}(k-1). \tag{23}$$

$P_{FC,max}$ is the maximum permissible FC power, $P_{FC,min}$ is the minimum permissible FC power, $P_{SC,max}$ is the maximum permissible SC power, $P_{SC,min}$ is the minimum permissible SC power, SOC_{max} is the maximum permissible value of SOC, SOC_{min} is the minimum permissible SOC, $\Delta P_{FC,max}$ is the maximum permissible rise rate power, and $\Delta P_{FC,min}$ is the maximum permissible fall rate power. The dynamic of the FC was limited to conservative values: $\Delta P_{FC,min} = -6\%$ and $\Delta P_{FC,max} = 4\%$ [15,39].

In this work, two EMSs were implemented. The first one is an adaptive Equivalent Consumption Minimization Strategy (ECMS), which is used during the sizing procedure. The second one is an optimal strategy, which is computed offline through deterministic dynamic programming [40] and is used to quantify the adequacy of the ECMS.

The ECMS is an online EMS based on local optimization, and its formulation has a connection with Pontryagin's minimum principle [41]. Assuming that the control input vector is $u = [\Delta P_{FC}, P_{br}]$, the local optimization can be expressed as:

$$\min_{u(k) \subseteq U(k)} \{LHV_{H_2} C_{H_2}(u(k)) + s(k) P_{SC}(u(k), k)\}, \tag{24}$$

where LHV_{H_2} is the Lower Heating Value of hydrogen ($LHV_{H_2} = 120\ kJ\ g^{-1}$) and $U(k)$ is the feasible set according to the constraints of the components expressed in (19)–(22). The first term in (24) quantifies the power from the primary power source, i.e., the FC, while the second one quantifies the power from the ESS. The equivalent factor, $s(k)$, is used to convert the electric-energy consumption to the equivalent hydrogen-energy consumption. In [41], different methods for computing $s(k)$ are described. In this work, an affine function dependent on the SOC was adopted:

$$s(k) = s_0 + s_1 (SOC_{ref} - SOC(k)), \tag{25}$$

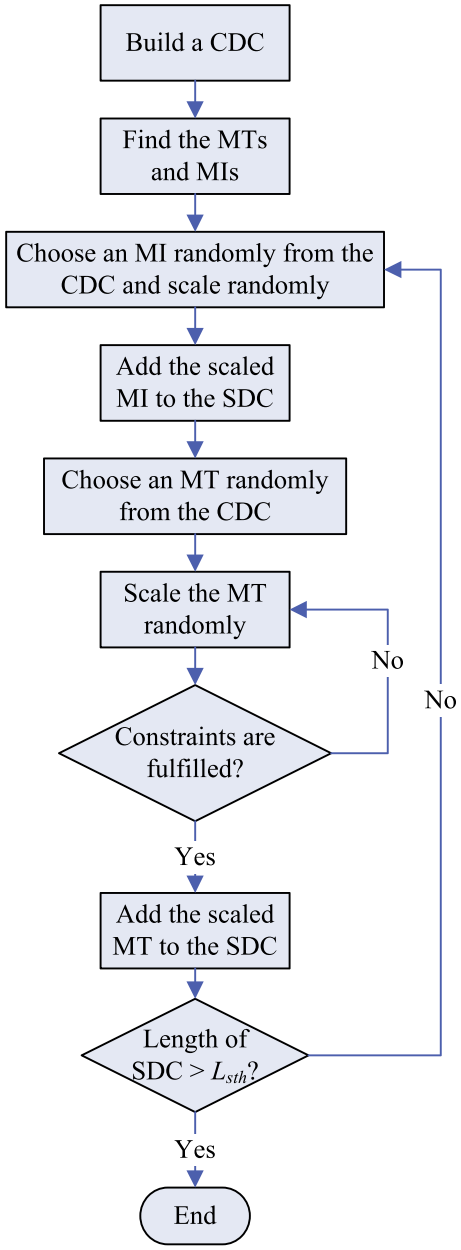

Fig. 4. Flow chart corresponding to the stochastic driving generation.

where SOC_{ref}, s_0, and s_1 are parameters that define the affine function. Fig. 7 is a graphical representation of (25). As observed, there are three adjustable parameters (SOC_{ref}, s_0, s_1). However, only two of them are required to represent the affine function. In this case, s_1 and s_0 are considered for adjustment, while SOC_{ref} is set equal to 0.7. In this type of HEV, the parameters selected for the ECMS have an important effect on both efficiency and drivability. There are no formal methods for finding the values of these parameters that produce a lower consumption to fulfil the power requirements. In this work, a parametric sweep was implemented, which is described in Section 5.

With regard to the implementation of dynamic programming to obtain an optimal strategy, hydrogen consumption is considered as a functional cost. Typical implementations of dynamic programming consider only the SOC as a state variable. However, in this case, to compute the constraint associated with the power rates of the FC, P_{FC} must also be considered as a state variable. Therefore, the state equations are the following:

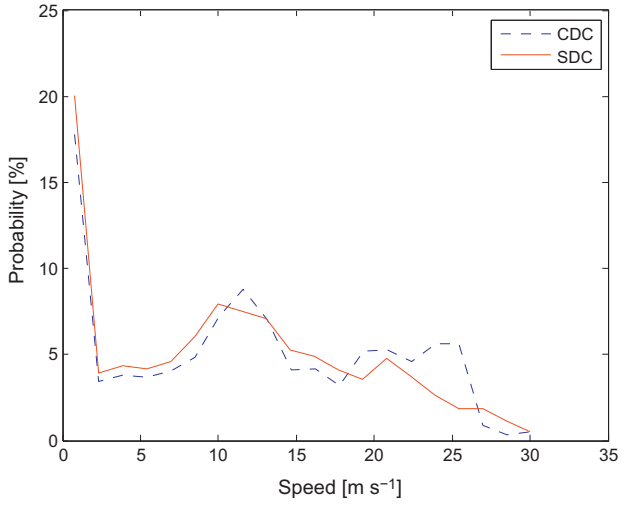

Fig. 5. Comparison of the speed probability diagrams for an SDC and CDC.

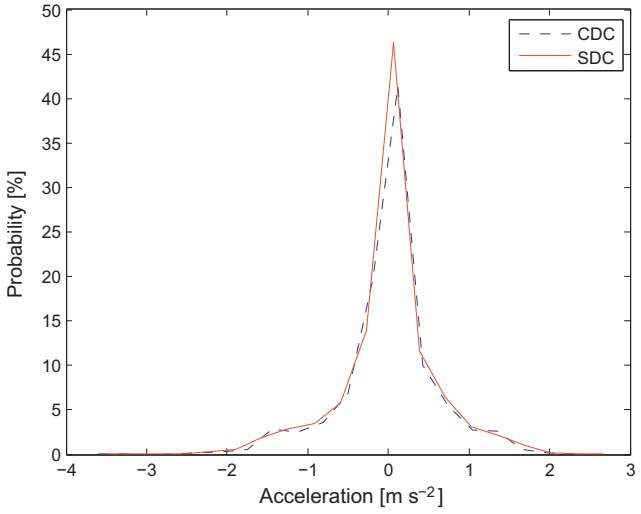

Fig. 6. Comparison of the acceleration probability diagram for an SDC and CDC.

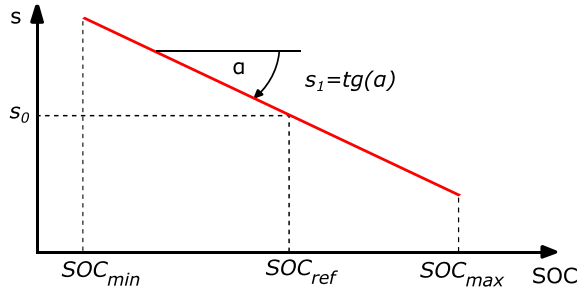

Fig. 7. Equivalent factor as a function of SOC.

$$\begin{cases} \mathrm{SOC}(k+1) = \mathrm{SOC}(k) + \Delta\mathrm{SOC}(k), \\ P_{\mathrm{FC}}(k+1) = P_{\mathrm{FC}}(k) + \Delta P_{\mathrm{FC}}(k), \end{cases} \tag{26}$$

where $\Delta\mathrm{SOC}(k)$ results from (13) and $\Delta P_{\mathrm{FC}}(k)$ is a control input variable. In summary, the optimization problem to be solved considers two state variables, (SOC and P_{FC}), and two control inputs, (ΔP_{FC} and P_{br}). Additionally, a sustained charge condition ($\mathrm{SOC}(0) = \mathrm{SOC}(L)$) is achieved through a final state constraint to avoid compensation for hydrogen consumption.

5. Sizing methodology

The size of the components in the powertrain is of great significance because size has a direct impact on system performance, efficiency and manufacturing cost. Insufficient component size means that the driving requirements cannot be met. Alternatively, a large size involves an unnecessary increase in the cost and mass. The sizing process is not trivial, since the speed profile is not known a priori and because the drivability is affected by the EMS. The objectives of optimal sizing are to determine the maximum power of the fuel cell ($P_{\mathrm{FC,max}}$) and the number of supercapacitors (N_{SC}) needed to: (i) meet the driving requirements; (ii) reduce hydrogen consumption; and (iii) reduce the installed power.

In this paper, a novel sizing methodology for FCHVs is presented. The sizing methodology is based on three tests: (i) Test 1: the fuel cell alone, without the supercapacitor bank, must be able to sustain a top speed v_{s1}; (ii) Test 2: the fuel cell alone, without the supercapacitor bank, must be able to sustain a speed v_{s2} with a constant slope in the road (α_s); and (iii) Test 3: the fuel cell together with the supercapacitor bank must be able to fulfil long-term SDC within a tolerance associated with speed compliance. The first two tests are used to determine the FC size, i.e., the value of $P_{\mathrm{FC,max}}$, while the third test is used to determine N_{SC}.

The speed compliance (C_v) in Test 3 is defined as follows:

$$C_v[\%] = \frac{(L - N_{ms})}{L} \times 100, \tag{27}$$

where N_{ms} is the number of missed-speed events during the driving cycle, and L is the total number of samples in the driving cycle. A value is considered a missed-speed event if the difference between the required and achieved speeds is greater than a given tolerance, δ_{v_t}.

The necessary FC power to support Test 1 can be derived from the power balance in (18), with $P_{\mathrm{SC}} = 0$ and $P_{br} = 0$:

$$P_{\mathrm{FC},1} = P_{req,1}/\eta_B, \tag{28}$$

where $P_{req,1}$ is set according to (12), which is computed for $v = v_{s1}$, $a = 0$, and $\alpha = 0$. P_{req} also depends on the vehicle mass, which is unknown at this point because it depends on the FC mass. However, the vehicle mass can be expressed as a function of the FC power from (10), assuming that $N_{\mathrm{SC}} = N_{\mathrm{SC,min}}$. Thus, $P_{\mathrm{FC},1}$ can be derived from (28). Similarly, the necessary FC power to support Test 2 can be derived from the following expression:

$$P_{\mathrm{FC},2} = P_{req,2}/\eta_B, \tag{29}$$

where $P_{req,2}$ is computed with $v = v_{s2}$, $a = 0$, and $\alpha = \alpha_s$. Then, the adopted $P_{\mathrm{FC,max}}$ is

$$P_{\mathrm{FC,max}} = \max\{P_{\mathrm{FC},1}, P_{\mathrm{FC},2}\}. \tag{30}$$

Once $P_{\mathrm{FC,max}}$ is determined, the drivability and efficiency of the FCHEV are evaluated in long-term SDC (Test 3). In this test, the size of the component and the EMS have a great influence. To find the optimal parameters of the ECMS, a parametric sweep was performed. The feasible solutions are those for which the number of missed-trace is lower than the tolerance C_{v_t}. Then, between the set of feasible solutions, those with minimal fuel consumption are chosen. This process is repeated for each N_{SC} proposed. The complete sizing methodology is summarized in Algorithm 1, while the parameters used for the described tests are collected in Table 3.

Finally, drivability can also be assessed on the basis of two widely known acceleration tests. The first computes the time required to accelerate from 0 to 100 km h^{-1}, while the second finds the time required to reach 1000 m starting from idle. From these tests, it may be concluded that with 13 supercapacitors or more (with the size of the fuel cell proposed), the energy available in the propulsion system is able to pass both tests.

Table 3
Parameters for drivability requirements.

Parameter	Value	Unit
v_{s1}	120	km h^{-1}
v_{s2}	80	km h^{-1}
α_s	6.5	%
δ_{ms}	5	%
C_{v_t}	95	%

In general, the optimal sizing of components is not trivial. In this case, the problem addressed has two objectives: reduce the fuel consumption and minimize the installed power. According to these objectives, a trade-off solution must be adopted. The results obtained by the described procedure are shown in Section 6.

Algorithm 1. Sizing methodology

Data: Load parameters of the FC, SC, and vehicle.
Define $N_{\mathrm{SC},min}$ and $N_{\mathrm{SC},max}$;
for $N_{SC} = N_{SC,min} : N_{SC,max}$ **do**
  Compute $P_{\mathrm{FC},1}$ and $P_{\mathrm{FC},2}$ from Eq. (28) and Eq. (29);
  $P_{\mathrm{FC},max} = \max\{P_{\mathrm{FC},1}, P_{\mathrm{FC},2}\}$;
  Compute m_v from Eq. (10);
  for $s_0 = s_{0,min} : \Delta s_0 : s_{0,max}$ **do**
    for $s_1 = s_{1,min} : \Delta s_1 : s_{1,max}$ **do**
      Run the vehicle under the SDC using ECMS;
      if $C_v \leq C_{v_t}$ **then**
        Save results
      end
    end
  end
end
Result: $P_{\mathrm{FC},max}$ and N_{SC}.

6. Results and discussion

In this section, the simulation results are presented to analyse the performance of the proposed sizing methodology. First, Algorithm 1 is executed from $N_{SC,\min} = 10$ to $N_{SC,\max} = 60$, where the lower limit corresponds to the minimum number of SC modules that fulfil the drivability requirement from Test 3. The results reveal that as N_{SC} increases, hydrogen consumption decreases. However, as N_{SC} increases there is an incremental rise in the total vehicle mass, the volume occupied by the ESS, and the cost. Therefore, there are two competing objectives: (i) to reduce the hydrogen consumption and (ii) to reduce N_{SC}.

The results derived from Algorithm 1 allow for a parametric sweep analysis, where the parameters s_0 and s_1 are varied according to Table 4. Fig. 8(a) shows the cloud of points corresponding to speed compliance. As mentioned in Section 5, a compliance of at least a 95% is required for drivability, and solutions below this line are considered infeasible. As expected, it can also be observed that the best-consumption solution line is close to 95% compliance. Alternately, Fig. 8(b) shows the effect of the number of SC modules on hydrogen consumption. In this figure, the feasible Pareto points and the Pareto front, which is the set of all Pareto-optimal points [42], can be observed, while the set of parameters s_0 and s_1 corresponding to the Pareto front is shown in Fig. 9. Notably, to conduct a proper analysis of the hydrogen consumed, it is necessary to account for the difference between SOC(0) and SOC(L). Additionally, it is useful to normalize hydrogen consumption with respect to the distance travelled along the driving cycle. Therefore, hydrogen consumption is computed as:

Table 4
ECMS parameters for the parametric sweep.

Parameter	Minimum	Maximum	Step
s_0	1	3	0.2
s_1	1	10	1

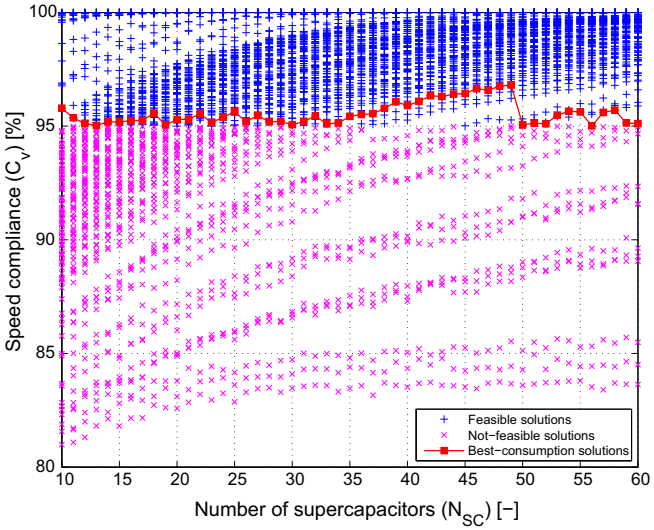

(a) Speed compliance.

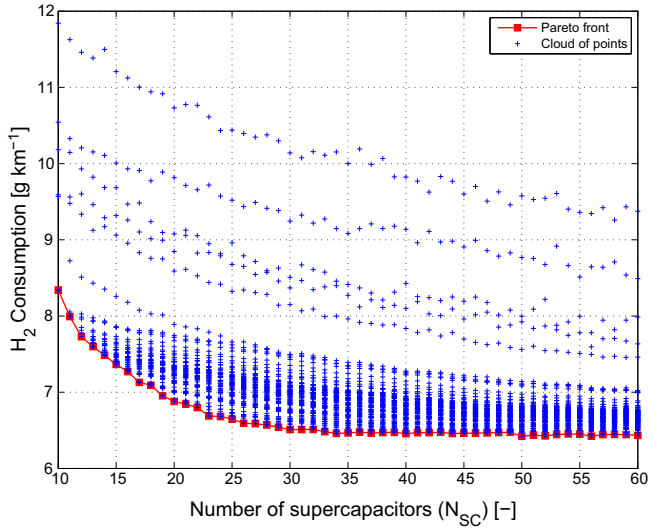

(b) Pareto consumption.

Fig. 8. Parametric sweep results.

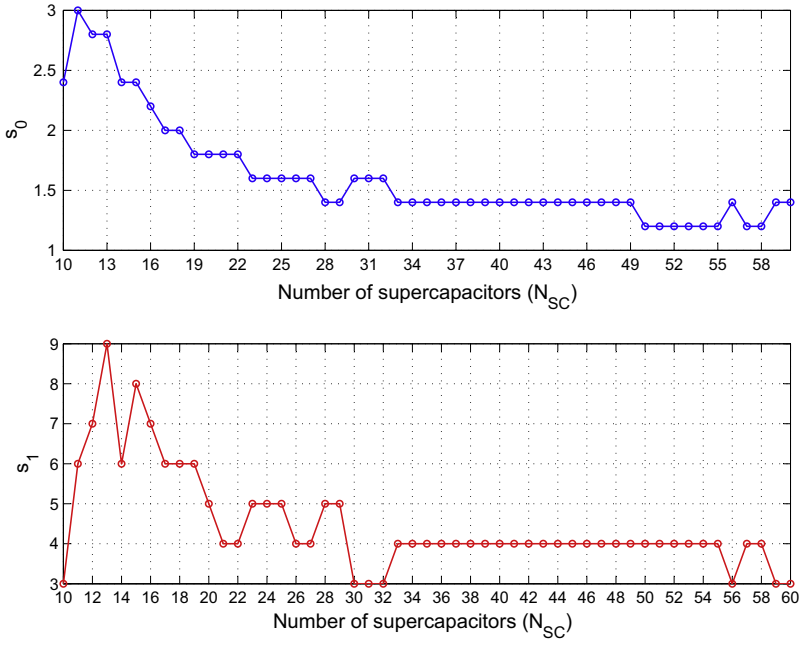

Fig. 9. Optimal parameters of ECMS.

$$H_{2,\,cons}\ [\mathrm{g\ km^{-1}}] = \frac{\sum_{k=0}^{L} C_{H_2}(k)\,\Delta t - (\mathrm{SOC}(L) - \mathrm{SOC}(0))\,k^*}{\sum_{k=0}^{L} v(k)\,\Delta t}, \tag{31}$$

with

$$k^* = \frac{E_{SC,\,bank}}{\mathrm{LHV}_{H_2}\,\eta_{FC}\,\eta_B\,\eta_{BB}\,\eta_{SC}}. \tag{32}$$

Regarding the achieved performance, it can be observed that, starting from $N_{SC} = 10$, a great reduction in hydrogen consumption is obtained as the number of SCs increases. In fact, a reduction of 22% is achieved from 10 to 34 SC modules. However, as N_{SC} increases, the hydrogen savings decrease until $N_{SC} = 34$, while the consumption remains approximately constant beyond this value. Note that these results are obtained using the ECMS.

To understand the causes of the reduction in hydrogen consumption for the proposed design, four relevant performance indicators are considered: the global propulsion efficiency, the brake to negative load ratio, the brake to hydrogen ratio, and the global FC efficiency.

The global propulsion efficiency is defined as follows:

$$\eta_{g,\,Prop} = \frac{\sum_{k=0}^{L} P_{load}^{(+)}(k)\,\Delta t}{\mathrm{LHV}_{H_2} \sum_{k=0}^{L} C_{H_2}(k)\,\Delta t}, \tag{33}$$

where $P_{load}^{(+)}$ is the positive load power:

$$P_{load}^{(+)}(k) = \begin{cases} P_{load}(k) & \text{if } P_{load}(k) > 0, \\ 0 & \text{otherwise.} \end{cases} \tag{34}$$

The numerator in (33) accounts for the total energy required to propel the vehicle, while the denominator accounts for the total energy of hydrogen consumed.

The brake to negative-load-power ratio is defined as:

$$\mathrm{Br/Load}^{(-)}[\%] = \frac{\sum_{k=0}^{L} P_{br}(k)\,\Delta t}{\sum_{k=0}^{L} P_{load}^{(-)}(k)\,\Delta t} \times 100, \tag{35}$$

where the numerator accounts for the total energy dissipated by the brakes and the denominator account for the total energy from negative load powers $\left(P_{load}^{(-)}\right)$:

$$P_{load}^{(-)}(k) = \begin{cases} P_{load}(k) & \text{if } P_{load}(k) < 0, \\ 0 & \text{otherwise.} \end{cases} \tag{36}$$

The brake-to-hydrogen ratio ($\mathrm{Br/H_2}$) is defined as the ratio between the energy dissipated via friction by the brakes and the total energy of hydrogen consumed in the cycle:

$$\mathrm{Br/H_2}[\%] = \frac{\sum_{k=0}^{L} P_{br}(k)\,\Delta t}{\mathrm{LHV}_{H_2} \sum_{k=0}^{L} C_{H_2}(k)\,\Delta t} \times 100. \tag{37}$$

Finally, the global efficiency of the FC is defined as:

$$\eta_{g,\,FC} = \frac{\sum_{k=0}^{L} P_{FC}(k)\,\Delta t}{\mathrm{LHV}_{H_2} \sum_{k=0}^{L} C_{H_2}(k)\,\Delta t}. \tag{38}$$

Fig. 10 shows the effect of N_{SC} on the previously defined performance indicators. Fig. 10(a) shows that the maximum global efficiency of the propulsion system is approximately 0.45, which is reached when $N_{SC} = 34$. Beyond this value, there is no improvement. Alternatively, it is well known that the use of friction brakes must be avoided and that regenerative braking must instead be used to improve global efficiency. However, when SOC_{max} or V_{max} are reached, the excess power has to be dissipated via friction brakes. As observed in Fig. 10(c), when N_{SC} is low, $\mathrm{Br/Load}^{(-)}$ is higher than 100%. This means that friction brakes dissipate power from the FC, which is undesirable. As a consequence, Fig. 10(b) shows that more than 10% of the energy from H_2 is consumed by friction brakes, whereas when $N_{SC} > 30$, $\mathrm{Br/H_2}$ is lower than 1%. Lastly, Fig. 10(d) shows that the increase in N_{SC} slightly reduces $\eta_{g,\,FC}$. Therefore, the results shown in Fig. 10 suggest that the reduction in hydrogen consumption is produced by the lower usage of friction brakes instead of higher global FC efficiency.

To analyse the performance of the ECMS, the results obtained using the optimal strategy were included in Fig. 11, combined with the Pareto front from Fig. 8(b). Notice that the greatest difference of the ECMS with respect to the optimal strategy is approximately 20% and it occurs when the number of SCs is low. In contrast, a difference of approximately 3% with respect to the optimal strategy is achieved when the number of SCs is large.

From the Pareto front in Fig. 11, a trade-off design can be adopted. Beyond $N_{SC} = 34$, there is no significant improvement in

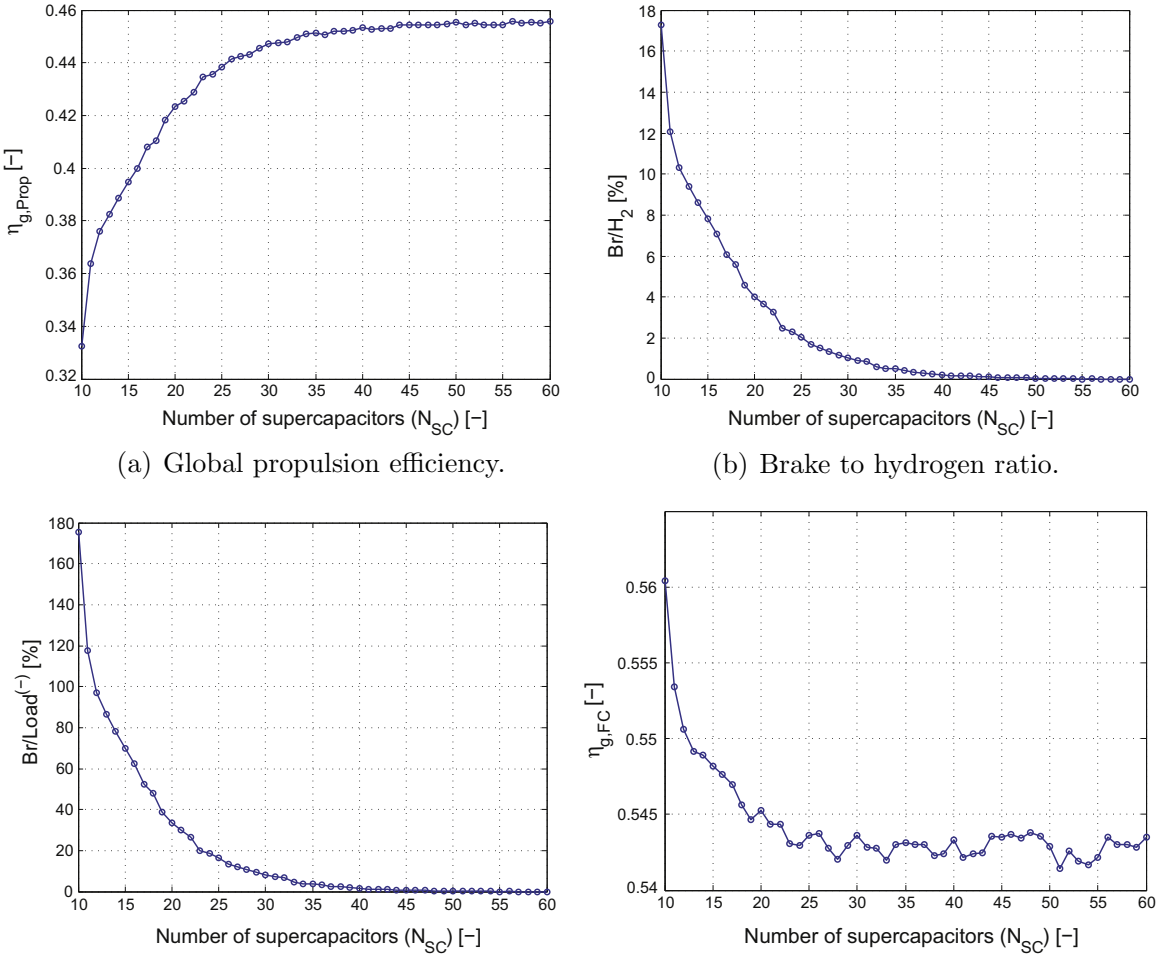

(a) Global propulsion efficiency.

(b) Brake to hydrogen ratio.

(c) Brake to negative-load-power ratio.

(d) Global FC efficiency.

Fig. 10. Performance indicators with increasing supercapacitor number.

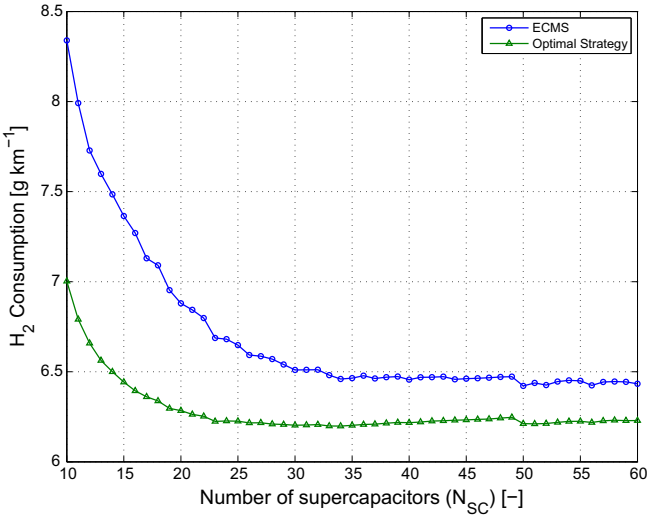

Fig. 11. Optimal and sub-optimal consumption.

hydrogen consumption. In fact, from $N_{SC} = 34$ to $N_{SC} = 50$, the reduction in hydrogen consumption is lower than 1%. Therefore, if $N_{SC} = 34$ is adopted, then $P_{FC,max} = 29.49$ kW. With regard to temporal behaviour, Fig. 12 shows a segment of select, relevant variables running on the SDC for the adopted size ($N_{SC} = 34, P_{FC,max} = 29.49$ kW), and the optimal parameters of the ECMS results $s_0 = 1.4$ and $s_1 = 4$, as observed in Fig. 9. In this figure, the real and reference speeds, the power split and the evolution of SOC can be observed. The difference between reference and real speeds is produced when the total maximum power available is lower than the power required. However, not all these differences are missed-speed traces, according to the definition in Section 5.

Once the size is adopted, the performance of the proposed design is evaluated under the CDC and compared with the SDC. The results are collected in Table 5. The table shows that the CDC requirement is also met by the design proposed. In addition, the consumption and the performance indicators under the CDC are close to those under the SDC. The results in this table, together with the results in Table 2, show that the characteristics of the SDC are similar to those of the CDC, not only in terms of speed and acceleration but also in terms of hydrogen consumption and drivability requirements.

Another sizing approach is analysed to compare the proposed methodology. In this new approach, the ECMS parameters remain fixed instead of being adjusted during the sizing procedure. According to Fig. 9, the set of parameters (s_0, s_1) that minimizes the H_2 consumption to meet the drivability requirement depends

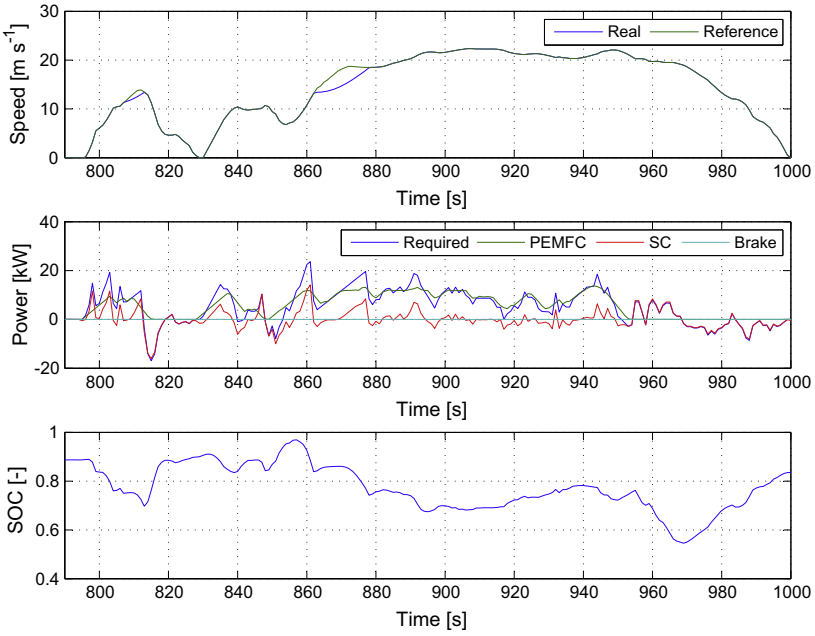

Fig. 12. Segment of the simulation running on the SDC with $N_{SC} = 34, s_0 = 1.4, s_1 = 4$, and $P_{FC,max} = 29.5$ kW.

Table 5
Simulation results using the ECMS with $N_{SC} = 34$, $s_0 = 1.4$, $s_1 = 4$, and $P_{FC,max} = 29.5$ kW.

	CDC	SDC
$H_{2\,cons}$ [g km^{-1}]	6.45	6.46
C_ν [%]	95.4	95.1
$\eta_{g,prop}$ [%]	45.3	45.1
Br/Load$^{(-)}$ [%]	1.93	3.79
Br/H$_2$ [%]	0.23	0.49
$\eta_{g,FC}$ [%]	54.5	54.3

Table 6
Design with $N_{SC} = 34$.

	$s_0 = 1.4$ $s_1 = 4$	$s_0 = 2$ $s_1 = 6$
C_ν [%]	95.1	97.2
$H_{2\,cons}$ [g km^{-1}]	6.45	6.69

Table 7
Design with $N_{SC} = 17$.

	$s_0 = 1.4$ $s_1 = 4$	$s_0 = 2$ $s_1 = 6$
C_ν [%]	89.7	95.6
$H_{2\,cons}$ [g km^{-1}]	–	7.13

on the number of SCs. For example, with $N_{SC} = 34$, the best parameters are $s_0 = 1.4$ and $s_1 = 4$, while with $N_{SC} = 17$ the best parameters are $s_0 = 2$ and $s_1 = 6$. To appreciate the effect of these parameters on vehicle performance, the design with $N_{SC} = 34$ is evaluated using ideal parameters of the design with $N_{SC} = 17$, and inversely, the design with $N_{SC} = 17$ is evaluated using ideal parameters of the design with $N_{SC} = 34$. The comparisons with the well-adjusted solutions are shown in Tables 6 and 7. As can be observed, with $N_{SC} = 34$, a bad EMS adjustment leads to an increase in consumption by 4%, with respect to the best solutions. Alternately, with $N_{SC} = 17$, a bad EMS adjustment leads to the infeasibility of the proposed design (the speed compliance is lower than 95%). These results highlight the advantage of the proposed methodology.

Finally, the size of the FC proposed is analysed. As observed in the sizing procedure, the size of the FC results from the first two tests. Such tests provide only the minimum FC size required to meet sustained speed conditions. For the purpose of reducing installed power, it seems correct to use this FC size. However, the size of the FC has effects on the efficiency map, the power rate limits, and the total vehicle mass. This suggests that the size of the FC affects global hydrogen consumption. To verify this presumption, various simulations with different oversized FCs were performed. Fig. 13 shows the hydrogen consumption obtained with the ECMS and the optimal strategy. According to the results using the ECMS, a minor reduction in the consumption is observed only when the number of supercapacitors is lower than 16. Otherwise, the consumption is increased. Alternately, when the optimal strategy is used, no improvements are observed upon oversizing the FC.

The increase in hydrogen consumption with respect to the size of the FC is produced by two causes: (i) an increase in the total vehicle mass and (ii) a reduction in the global efficiency of the powertrain. The increase in the total mass is only 3% when the size of the FC is increased by 40%, while the reduction in the global efficiency is 1.5%, as can be observed in Fig. 14. To aid the understanding of such behaviour, Fig. 15 shows the brake to negative-load-power ratio and the global FC efficiency.

Finally, as a conclusion of the oversizing FC analysis, when N_{SC} is low, the reduction in the hydrogen consumption as result of increasing FC size is due to a reduction in the usage of friction brakes. However, when N_{SC} is increased this effect disappears, and the higher consumption is due to a lower global FC efficiency.

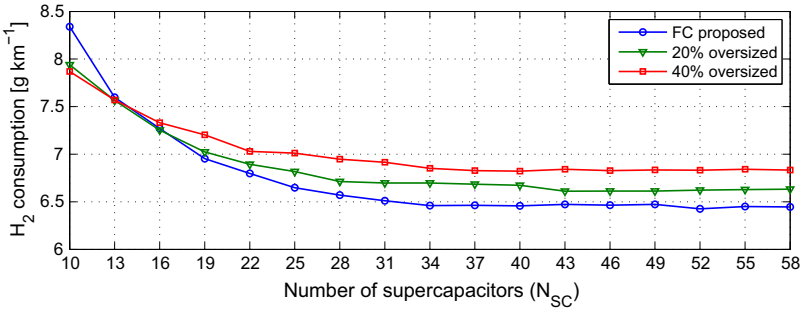

(a) ECMS

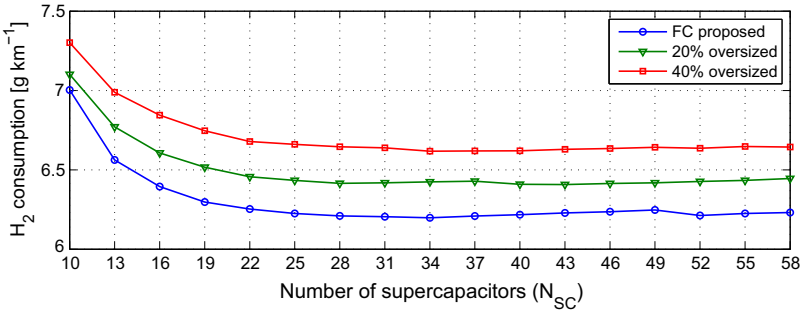

(b) Optimal Strategy

Fig. 13. Consumption with an oversized FC.

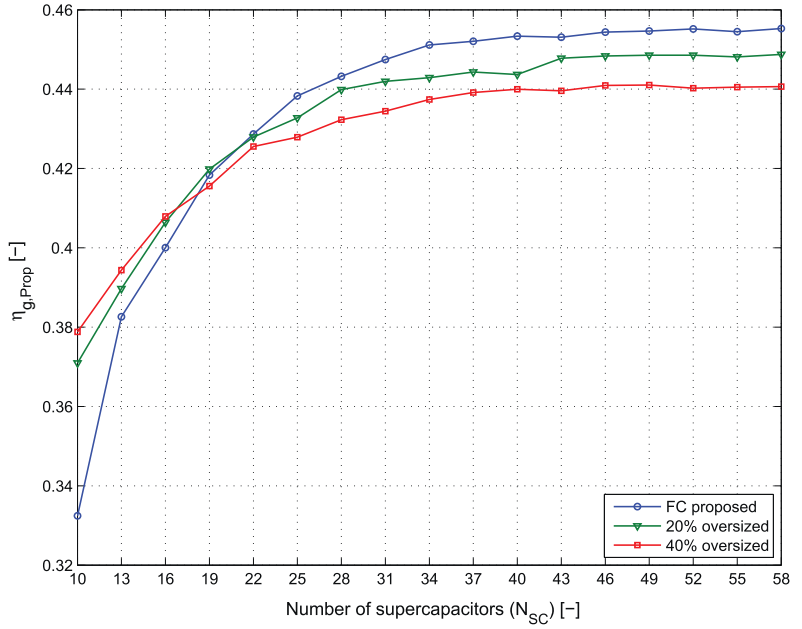

Fig. 14. Global efficiency of propulsion system ($\eta_{g,Prop}$).

7. Conclusions

This paper addresses the sizing and performance analysis of fuel cell/supercapacitor hybrid vehicles. In this sense, a comprehensive and innovative approach was presented. The sizing methodology proposed is based on static and dynamic driving conditions. The dynamic driving conditions were provided by a long-term stochastic driving cycle, which was generated through a novel methodology based on standard driving cycles. The performance of the FCHV in the long-term driving cycle was evaluated using the ECMS as energy management. A parametric sweep performed during the sizing procedure allowed the ideal parameters of the strategy to be identified for each sizing that was proposed. After the sizing procedure, the performance of the FCHV was also evaluated under the optimal offline strategy, computed using Dynamic Programming.

The results obtained with the sizing procedure show that the evolution of hydrogen consumption with respect to the number

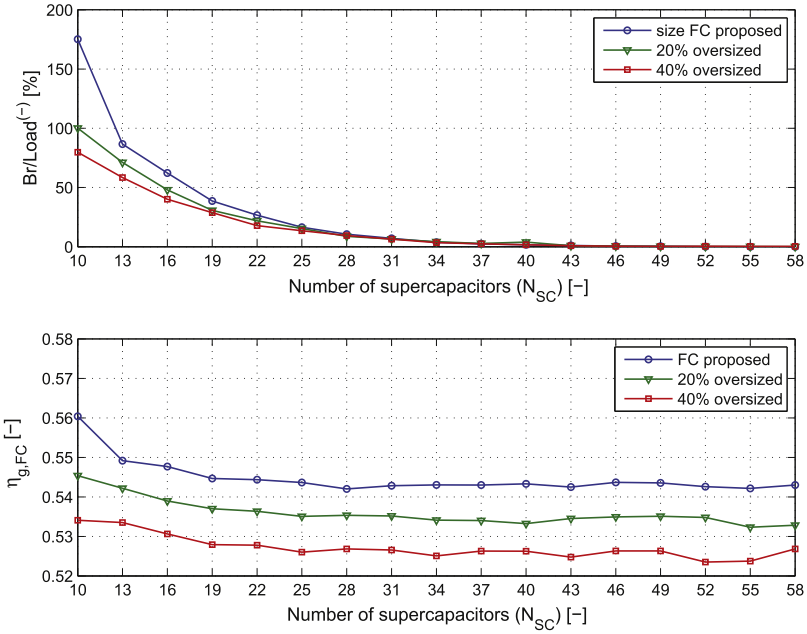

Fig. 15. Brake to negative-load-power ratio ($Br/Load^{(-)}$) and global efficiency of the FC ($\eta_{g,FC}$).

of supercapacitors converges slowly to a minimum. This suggests that it is better to adopt a trade-off solution, instead of the solution corresponding to minimum consumption. Moreover, the analysis of the proposed performance indicators showed that as the number of supercapacitors increases the usage of friction brakes decreases, which significantly reduces hydrogen consumption. With respect to the FC, the size proposed by this methodology achieves lower hydrogen consumption compared to the FCHV with a larger FC size. Indeed, it was observed that the incremental rise in hydrogen consumption is due to both the increase of total vehicle mass and a reduction in the global fuel cell efficiency. Additionally, the performance of the real-time ECMS in comparison with the off-line optimal strategy exhibited a significant difference in hydrogen consumption with a low number of supercapacitors. However, this difference is reduced as the number of supercapacitors is increased. In addition, the high sensibility of this class of vehicle to the EMS and the importance of adjusting the EMS parameters in the sizing procedure have been verified by simulation. Finally, it is worth mentioning that despite the results being focused on a specific light car, the methodology presented in this paper is general enough to cover a wide range of problems concerning the sizing of components in FCHVs.

Acknowledgments

The authors thank the financial support from CONICET, UNR-FCEIA, and ANPCYT (PICT 2014-1607).

References

[1] Bizon N. On tracking robustness in adaptive extremum seeking control of the fuel cell power plants. Appl Energy 2010;87:3115–30.
[2] Hung Y, Wu C. An integrated optimization approach for a hybrid energy system in electric vehicles. Appl Energy 2012;98:479–90.
[3] Ahluwalia R, Wang X, Rousseau A. Fuel economy of hybrid fuel-cell vehicles. J Power Sources 2005;152:233–44.
[4] Feroldi D, Serra M, Riera J. Design and analysis of fuel-cell hybrid systems oriented to automotive applications. IEEE Trans Vehic Technol 2009;58:4720–9.
[5] Liu C, Liu L. Optimal power source sizing of fuel cell hybrid vehicles based on Pontryagin's minimum principle. Int J Hydrogen Energy 2015;40:8454–64.
[6] Ettihir K, Boulon L, Agbossou K. Optimization-based energy management strategy for a fuel cell/battery hybrid power system. Appl Energy 2016;163:142–53.
[7] Xu L, Mueller C, Li J, Ouyang M, Hu Z. Multi-objective component sizing based on optimal energy management strategy of fuel cell electric vehicles. Appl Energy 2015;157:664–74.
[8] Eren Y, Gorgun H. An applied methodology for multi-objective optimum sizing of hybrid electric vehicle components. Int J Hydrogen Energy 2015;40:2312–9.
[9] Xu L, Ouyang M, Li J, Yang F, Lu L, Hua J. Optimal sizing of plug-in fuel cell electric vehicles using models of vehicle performance and system cost. Appl Energy 2013;103:477–87.
[10] Herrera V, Milo A, Gaztañaga H, Etxeberria-Otadui I, Villarreal I, Camblong H. Adaptive energy management strategy and optimal sizing applied on a battery-supercapacitor based tramway. Appl Energy 2016;169:831–45.
[11] Hu X, Murgovski N, Johannesson L, Egardt B. Optimal dimensioning and power management of a fuel cell/battery hybrid bus via convex programming. IEEE/ASME Trans Mechatron 2015;20:457–68.
[12] Hu X, Johannesson L, Murgovski N, Egardt B. Longevity-conscious dimensioning and power management of the hybrid energy storage system in a fuel cell hybrid electric bus. Appl Energy 2015;137:913–24.
[13] Tie S, Tan C. A review of energy sources and energy management system in electric vehicles. Renew Sustain Energy Rev 2013;20:82–102.
[14] Sulaiman N, Hannan M, Mohamed A, Majlan E, Daud W. A review on energy management system for fuel cell hybrid electric vehicle: issues and challenges. Renew Sustain Energy Rev 2015;52:802–14.
[15] Rodatz P, Paganelli G, Sciarretta A, Guzzella L. Optimal power management of an experimental fuel cell/supercapacitor-powered hybrid vehicle. Control Eng Pract 2015;13:41–53.
[16] Pérez L, De Angelo C, Pereyra V. Determination of the equivalent consumption in hybrid electric vehicles in the state-constrained case. Oil Gas Sci Technol 2016;71:30.
[17] Tazelaar E, Veenhuizen B, van den Bosch P, Grimminck M. Analytical solution of the energy management for fuel cell hybrid propulsion systems. IEEE Trans Vehic Technol 2012;61:1986–98.
[18] Arce A, del Real A, Bordons C. MPC for battery/fuel cell hybrid vehicles including fuel cell dynamics and battery performance improvement. J Process Control 2009;19:1289–304.
[19] Lee C, Lin W. Stochastic self-optimizing power management for fuel cell hybrid scooters of different sized components. Int J Hydrogen Energy 2015;40:5197–209.
[20] Fares D, Chedid R, Panik F, Karaki S, Jabr R. Dynamic programming technique for optimizing fuel cell hybrid vehicles. Int J Hydrogen Energy 2015;40:7777–90.
[21] Feroldi D, Serra M, Riera J. Energy management strategies based on efficiency map for fuel cell hybrid vehicles. J Power Sources 2009;190:387–401.
[22] Trovão J, Pereirinha P, Jorge H, Antunes C. A multi-level energy management system for multi-source electric vehicles–an integrated rule-based meta-heuristic approach. Appl Energy 2013;105:304–18.
[23] Song Z, Hofmann H, Li J, Hou J, Han X, Ouyang M. Energy management strategies comparison for electric vehicles with hybrid energy storage system. Appl Energy 2014;134:321–31.

[24] Castaings A, Lhomme W, Trigui R, Bouscayrol A. Comparison of energy management strategies of a battery/supercapacitors system for electric vehicle under real-time constraints. Appl Energy 2016;163:190–200.
[25] Hwang J, Chen Y, Kuo J. The study on the power management system in a fuel cell hybrid vehicle. Int J Hydrogen Energy 2012;37:4476–89.
[26] Thounthong P, Raël S, Davat B. Control algorithm of fuel cell and batteries for distributed generation system. IEEE Trans Energy Convers 2008;23:148–55.
[27] Torreglosa J, Jurado F, García P, Fernández L. Application of cascade and fuzzy logic based control in a model of a fuel-cell hybrid tramway. Eng Appl Artif Intell 2011;24:1–11.
[28] Ferreira A, Pomilio J, Spiazzi G, de Araujo Silva L. Energy management fuzzy logic supervisory for electric vehicle power supplies system. IEEE Trans Power Electron 2008;23:107–15.
[29] Kisacikoglu M, Uzunoglu M, Alam M. Load sharing using fuzzy logic control in a fuel cell/ultracapacitor hybrid vehicle. Int J Hydrogen Energy 2009;34:1497–507.
[30] National Renewable Energy Laboratory (NREL). Advanced Vehicle Simulator (ADVISOR); 2015. <http://www.nrel.gov/transportation/systems_analysis_tools.html>.
[31] Song Z, Li J, Han X, Xu L, Lu L, Ouyang M, et al. Multi-objective optimization of a semi-active battery/supercapacitor energy storage system for electric vehicles. Appl Energy 2014;135:212–24.
[32] Ouyang M, Zhang W, Wang E, Yang F, Li J, Li Z, et al. Performance analysis of a novel coaxial power-split hybrid powertrain using a CNG engine and supercapacitors. Appl Energy 2015;157:595–606.
[33] Schwarzer V, Ghorbani R. Drive cycle generation for design optimization of electric vehicles. IEEE Trans Vehic Technol 2013;62:89–97.
[34] Ravey A, Watrin N, Blunier B, Bouquain D, Miraoui A. Energy-source-sizing methodology for hybrid fuel cell vehicles based on statistical description of driving cycles. IEEE Trans Vehic Technol 2011;60:4164–74.
[35] Wang H, Zhang X, Ouyang M. Energy consumption of electric vehicles based on real-world driving patterns: a case study of Beijing. Appl Energy 2015;157:710–9.
[36] DieselNet. Emission test cycles; 2005. http://www.dieselnet.com.
[37] Dembski N, Guezennec Y, Soliman A. Analysis and experimental refinement of real-world driving cycles. SAE 2002-01-0069.
[38] Ho S, Wong Y, Chang V. Developing Singapore driving cycle for passenger cars to estimate fuel consumption and vehicular emissions. Atmos Environ 2014;97:353–62.
[39] Valverde L, Bordons C, Rosa F. Integration of fuel cell technologies in renewable-energy-based microgrids optimizing operational costs and durability. IEEE Trans Ind Electron 2016;63:167–77.
[40] Kirk D. Optimal control theory: an introduction. New York: Courier Corporation; 2012.
[41] Guzzella L, Sciarretta A. Vehicle propulsion systems. London: Springer; 2007.
[42] Na W, Gou B. The efficient and economic design of PEM fuel cell systems by multi-objective optimization. J Power Sources 2007;166:411–8.